THE JOURNAL OF BIOLOGICAL CHEMISTRY Vol. 279, No. 24, Issue of June 11, pp. 25789–25797, 2004
Printed in U.S.A.

Crystal Structure and Mutational Analysis of Heparan Sulfate 3-*O*-Sulfotransferase Isoform 1*

Received for publication, January 30, 2004, and in revised form, March 10, 2004
Published, JBC Papers in Press, April 1, 2004, DOI 10.1074/jbc.M401089200

Suzanne C. Edavettal‡, Karen A. Lee§, Masahiko Negishi¶, Robert J. Linhardt‖, Jian Liu‡, and Lars C. Pedersen§**

From the ‡Division of Medicinal Chemistry and Natural Products, School of Pharmacy, University of North Carolina, Chapel Hill, North Carolina 27599, §Laboratory of Structural Biology and ¶Laboratory of Reproductive and Developmental Toxicology, NIEHS, National Institutes of Health, Research Triangle Park, North Carolina 27709, and ‖Department of Chemistry and Chemical Biology, Rensselaer Polytechnic Institute, Troy, New York 12180

Heparan sulfate interacts with antithrombin, a protease inhibitor, to regulate blood coagulation. Heparan sulfate 3-*O*-sulfotransferase isoform 1 performs the crucial last step modification in the biosynthesis of anticoagulant heparan sulfate. This enzyme transfers the sulfuryl group (SO_3) from 3′-phosphoadenosine 5′-phosphosulfate to the 3-OH position of a glucosamine residue to form the 3-*O*-sulfo glucosamine, a structural motif critical for binding of heparan sulfate to antithrombin. In this study, we report the crystal structure of 3-*O*-sulfotransferase isoform 1 at 2.5-Å resolution in a binary complex with 3′-phosphoadenosine 5′-phosphate. This structure reveals residues critical for 3′-phosphoadenosine 5′-phosphosulfate binding and suggests residues required for the binding of heparan sulfate. In addition, site-directed mutagenesis analyses suggest that residues Arg-67, Lys-68, Arg-72, Glu-90, His-92, Asp-95, Lys-123, and Arg-276 are essential for enzymatic activity. Among these essential amino acid residues, we find that residues Arg-67, Arg-72, His-92, and Asp-95 are conserved in heparan sulfate 3-*O*-sulfotransferases but not in heparan *N*-deacetylase/*N*-sulfotransferase, suggesting a role for these residues in conferring substrate specificity. Results from this study provide information essential for understanding the biosynthesis of anticoagulant heparan sulfate and the general mechanism of action of heparan sulfate sulfotransferases.

Heparan sulfate (HS)[1] is widely expressed in animal and human tissues. It has diverse roles in development, assisting viral infections, and homeostasis (1–3). HS is a highly sulfated polysaccharide consisting of 1–4-linked sulfated glucosamine and sulfated glucuronic/iduronic acid residues. The specific sequences of sulfated saccharide in HS determine its various functions.

Synthesis of biologically active HS is accomplished through a complex biosynthetic pathway. HS is initially synthesized as a copolymer of glucuronic acid and *N*-acetylated glucosamine by D-glucuronyl and *N*-acetyl-D-glucosaminyltransferase followed by various modifications in the Golgi apparatus (4). These modifications include *N*-deacetylation and *N*-sulfonation of glucosamine, C_5 epimerization of glucuronic acid to form iduronic acid residues, and 2-*O*-sulfonation of iduronic and glucuronic acid residues as well as 6-*O*-sulfonation and 3-*O*-sulfonation of the glucosamine units. The stepwise sulfonation reactions are illustrated in Fig. 1. All of the enzymes that are responsible for the biosynthesis of HS have been cloned and characterized (5).

The blood coagulation pathway is composed of a cascade of proteolytic reactions ultimately generating fibrin thrombi. The proanticoagulant activity of this cascade is balanced by several natural anticoagulant mechanisms. Binding of HS to antithrombin (AT) represents the most important of these mechanisms. HS achieves its anticoagulant activity by interacting with AT, which undergoes a conformation change, generating the active form of AT to inhibit blood coagulation factors Xa and thrombin. This anticoagulant process prevents the formation of deleterious blood clots. Heparin, a specialized HS found in mast cells, is the most commonly used anticoagulant drug.

Anticoagulant HS and heparin contain structurally defined AT binding pentasaccharide sequences with the structure, -GlcNS(or Ac)6S-GlcUA-GlcNS3S±6S-IdoUA2S-GlcNS6S- (GlcUA is glucuronic, and IdoUA is iduronic acid) (Fig. 1) (6). The 3-*O*-sulfo glucosamine unit (GlcNS3S±6S) in this binding site is essential for interaction with AT. The lack of a 3-*O*-sulfo group in this unit decreases AT binding affinity by 18,000-fold (6). A recently approved anticoagulant drug, Arixtra, prepared by organic synthesis is based on this pentasaccharide scaffold. The recently reported enzymatic synthesis of a similar pentasaccharide utilizes 3-OST-1 in the last modification step (5) and opens up a new approach to preparation of such anticoagulants.

The essential physiological role of 3-*O*-sulfo HS (or anticoagulant HS) in blood coagulation is best demonstrated through the study of AT and AT mutants. A severe thrombosis phenotype is observed in mice carrying an AT mutant defective in heparin binding, suggesting a key role for HS-AT interaction in balancing procoagulant and anticoagulant activities *in vivo* (7). Additionally, patients with AT mutants defective in heparin and HS binding suffer from thrombosis (8–10). Furthermore, it appears that complete ablation of AT-HS binding is required to

* This work was supported in part by National Institutes of Health Grant AI50050 (to J. L.) and American Heart Association Mid-Atlantic Affiliate Grant-in-aid 0355800U (to J. L.). The costs of publication of this article were defrayed in part by the payment of page charges. This article must therefore be hereby marked "*advertisement*" in accordance with 18 U.S.C. Section 1734 solely to indicate this fact.

The atomic coordinates and structure factors (code 1S6T) have been deposited in the Protein Data Bank, Research Collaboratory for Structural Bioinformatics, Rutgers University, New Brunswick, NJ (http://www.rcsb.org/).

** To whom correspondence and reprint requests should be addressed: Rm. 309, Beard Hall, University of North Carolina, Chapel Hill, NC 27599. Tel: 919-843-6511; Fax: 919-843-5432; E-mail: jian_liu@unc.edu.

[1] The abbreviations used are: HS, heparan sulfate; AT, antithrombin; 3-OST, 3-*O*-sulfotransferase; PAPS, 3′-phosphoadenosine 5′-phosphosulfate; PAP, 3′-phosphoadenosine 5′-phosphate; PSB, phosphosulfate binding; NST-1, *N*-deacetylase/*N*-sulfotransferase; Tricine, *N*-[2-hydroxy-1,1-bis(hydroxymethyl)ethyl]glycine; ITC, isothermal titration calorimetry; MOPS, 4-morpholinepropanesulfonic acid; WT, wild type.

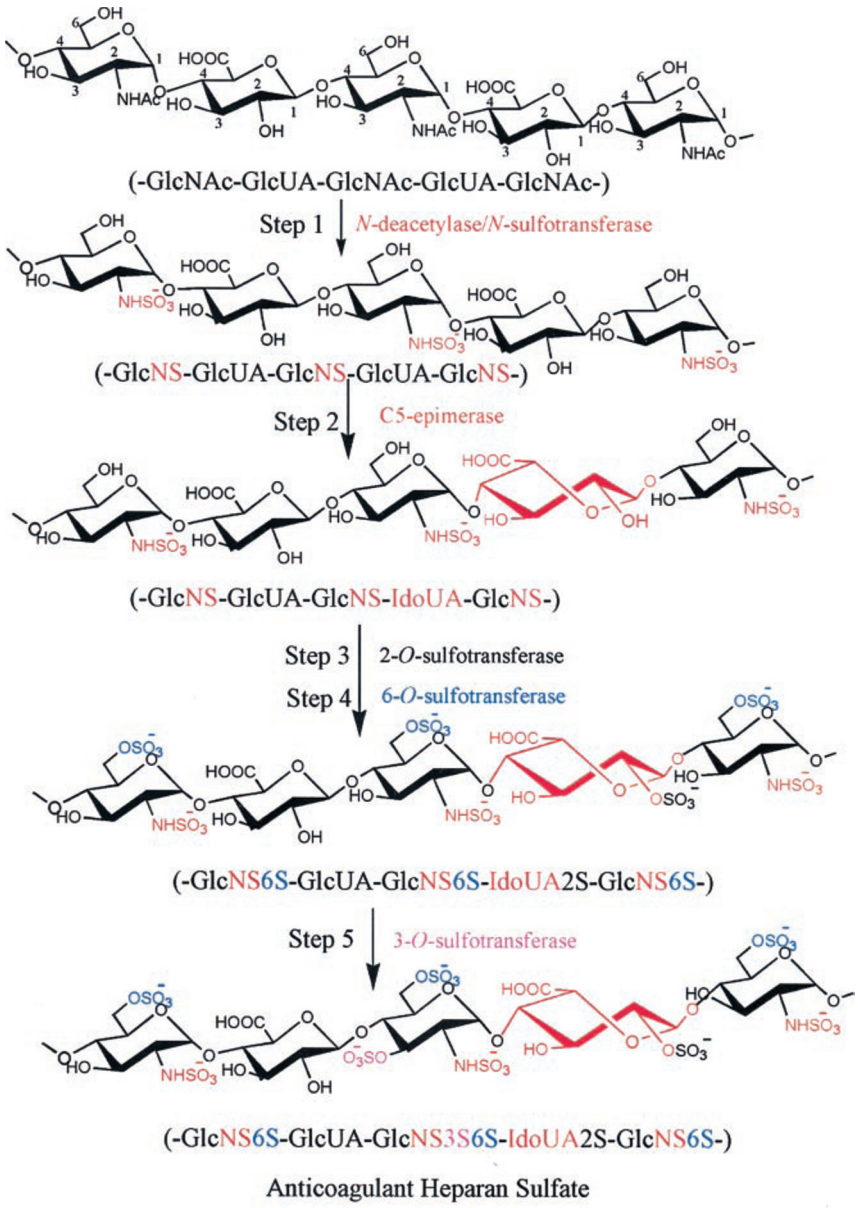

FIG. 1. **The schematic biosynthesis of anticoagulant heparan sulfate.** Five steps are involved in the biosynthesis of HS after the polysaccharide backbone is made. The *numbers* indicate the positions of each sugar unit. Both *N*-deacetylase/*N*-sulfotransferase and C_5-epimerase modifications are indicated in *red*. The 2-*O*-sulfotransferase and 6-*O*-sulfotransferase modifications are indicated in *black* and *blue*, respectively. The 3-*O*-sulfotransferase modification is indicated in *purple*. For clarity, we have indicated the 3-*O*-sulfotransferase isoform 1 modifications only in this figure. *GlcUA*, glucuronic; *IdoUA*, iduronic acid; *Glc*, glucosamine.

reveal the full physiological role of anticoagulant HS *in vivo* (11). The final step in the biosynthesis of anticoagulant HS can be catalyzed by either 3-OST-1 or 3-OST-5 isoforms (12, 13). Gene redundancy in the biosynthesis of anticoagulant HS helps to explain why 3-OST-1 knockout mice failed to exhibit a prothrombotic phenotype (14).

Heparan sulfate 3-*O*-sulfotransferase (3-OST) is present in at least six different isoforms that have unique expression patterns in human tissues (15, 16). The amino acid sequences of the different isoforms have 50–80% homology in their sulfotransferase domains (15). These different 3-OST isoforms transfer sulfuryl groups to the 3-OH position of glucosamine units residing within the context of different saccharide sequences. As a result, the HS products generated by these different isoforms exhibit unique and distinctive biological activities. It is known that HS modified by 3-OST-1 and 3-OST-5 display anticoagulant activity, whereas HS modified by 3-OST-3 and 3-OST-5 serve as entry receptors for herpes simplex virus-1 (12, 16, 17). The structural features of 3-OST isoforms that dictate substrate specificity are currently unknown.

The sulfotransferase family can be organized into two categories based on the sub-cellular localizations; they are cytosolic and Golgi sulfotransferases (18, 19). The crystal structures of different sulfotransferases reveal structural similarity in their PAPS binding sites between the cytosolic and Golgi sulfotransferases, suggesting that different sulfotransferases probably follow similar mechanisms in the transfer of the sulfuryl group even though they exhibit high selectivity in substrate binding (20, 21). The structures of a number of cytosolic sulfotransferases complexed with acceptor substrates have been solved, providing clues that have led to a better understanding of their catalytic mechanism and mode of substrate recognition (22–24). HS sulfotransferases are considered to be Golgi sulfotransferases. The crystal structure of the binary complex of the sulfotransferase domain of the HS *N*-deacetylase/*N*-sulfotransferase (NST-1) and 3′-phosphoadenosine 5′-phosphate (PAP) was solved by Kakuta *et al.* (21). This represents the first and only structure of a HS sulfotransferase previously determined.

In this study, we report the crystal structure of a binary complex of mouse 3-OST-1 and PAP. The structure of this enzyme is very similar to NST-1 but with unique structural features in the HS binding cleft. Results from mutational analysis of amino acid residues at and around the active site in

TABLE I
Crystallographic data statistics

Data set	3-OST-1 (high)		3-OST-1 (low)
Unit cell dimensions	$a = b = 300.14$ $c = 84.20$ $\alpha = \beta = \gamma = 90°$		$a = b = 298.69$ $c = 83.82$ $\alpha = \beta = \gamma = 90°$
Space group	I4 (1) 22		I4 (1) 22
No. of observations	741,873		180,101
Unique reflections	63,928		43,945
R_{sym} (%) (last shell)[a]	11.6 (37.1)		13.7 (61.5)
$I/\sigma I$ (last shell)	7.4 (1.7)		6.7 (1.4)
Mosaicity	0.41		0.62
Completeness (%) (last shell)	96.7 (83.6)		93.9 (82.4)
Refinement statistics			
Resolution (Å)	25.0–2.5		25.0–2.8
R_{cryst} (%)[b]	24.3		
R_{free} (%)[c]	26.4		
No. of water	178		
Mean B value (Å)	58.3		
For:	Complex A	Complex B	Complex C
Protein	43.06	39.17	100.69
PAP	31.23	33.18	69.76
Root mean square deviation from ideal values[d]			
Bond length (Å)	0.009		
Bond angle (°)	1.4		
Dihedral angle (°)	22.4		
Improper angle (°)	0.95		
Ramachandran statistics			
94.57% residues are in favored (98%) regions			
99.74% residues are in allowed (>99.8%) regions[e]			

[a] $R_{sym} = \Sigma\ (|I_i - \langle I\rangle|)/\Sigma(I_i)$ where I_i is the intensity of the Ith observation, and $\langle I\rangle$ is the mean intensity of the reflection.
[b] $R_{cryst} = \Sigma||F_o| - |F_o||\Sigma|F_o|$ calculated from working data set.
[c] R_{free} was calculated from 5% of data randomly chosen not to be included in refinement.
[d] Ramachandran results were determined by MolProbity.
[e] Two residues from complex C, which lie outside this region, are in allowed regions based on PROCHECK (28).

3-OST-1 reveal a series of amino acid residues that is critical for sulfotransferase activity. These results, when combined with a structural alignment to NST-1 and sequence alignments to other isoforms of 3-OST, provide insight into the role certain residues may play in catalysis and dictating substrate specificity for these HS sulfotransferases.

EXPERIMENTAL PROCEDURES

Materials—Full-length mouse 3-OST-1 cDNA (m3-OST-1-pcDNA3) was purified from a mouse L-cell cDNA library (25). [^{35}S]PAPS was prepared by incubating 0.4–2 mCi/ml [^{35}S]Na_2SO_4 (carrier-free, MP Biomedical) and 16 mM ATP with 5 mg/ml dialyzed yeast extract (Sigma) (26). HS from bovine kidney was purchased from MP Biomedical (Irvine, CA). PAP was purchased from Sigma.

Expression, Purification, and Crystallization of 3-OST-1

Preparation of 3-OST-1 Bacterial Expression Plasmid (b3-OST-1-pET28)—The cDNA fragment encoding the catalytic domain of 3-OST-1 (G48-H311) was amplified from m3-OST-1-pcDNA3 with a 5′ overhang containing an NdeI site and a 3′ overhang containing an EcoRI site. This construct was inserted into the pET28a vector (Novagen) using the NdeI and EcoRI restriction sites to produce a His_6-tagged protein. The resultant plasmid (b3-OST-1-pET28) was sequenced to confirm the reading frame and the lack of mutations within the coding region (University of North Carolina, DNA sequencing core facility). The plasmid, b3-OST-1-pET28, was transformed into BL21(DE3)RIL cells (Stratagene) for the expression of 3-OST-1.

Protein Expression and Purification—Cells containing the b3-OST-1-pET28 were grown in 12 2.8-liter Fernbach flasks containing 1 liter of LB media with 50 μg/ml kanamycin at 37 °C. When the A_{600} reached 0.6–0.8, the temperature was lowered to 22 °C for 15 min. Isopropyl-β-D-thiogalactopyranoside was then added to a final concentration of 200 μM, and the cells were allowed to shake overnight. Cells were pelleted and resuspended in 120 ml of sonication buffer, 25 mM Tris, pH 7.5, 500 mM NaCl, and 10 mM imidazole. Cells were disrupted by sonication then spun down. The supernatant was applied to nickel nitrilotriacetic acid-agarose resin (Qiagen) in batch and washed with sonication buffer. The resin was loaded onto a column, and the protein was eluted with an imidazole gradient from 10 to 250 mM. The protein was dialyzed then concentrated to 16 mg/ml in 20 mM Tris, pH 7.5, 100 mM NaCl, and 4 mM PAP. A total of 28 mg of protein was obtained.

Protein Crystallization and Structure Solution—Crystals of 3-OST-1 were grown using the hanging drop method at 4 °C by mixing 2 μl of the protein solution with 2 μl of the reservoir solution containing 0.1 M citrate, pH 5.5, and 11% polyethylene glycol 4000. Before data collection, crystals were transferred to a solution containing 0.1 M citrate, pH 5.5, 20% polyethylene glycol 4000, 0.1 M NaCl, 4 mM PAP, and 12.5% ethylene glycol. The crystals were mounted in a loop and flash-frozen in liquid nitrogen. Data were collected at −180 °C on a RaxisIV area detector for the low resolution data set. A high resolution data set was collected on another crystal at the Advanced Photon Source on SER-CAT beamline 22 using a MAR225 area detector. Both data sets were processed using HKL2000 (Table I) (27). A model of NST-1 (21) consisting of residues 603–632, 642–664, 670–736, 744–868, and PAP was used as a search molecule for molecular replacement using Molrep in CCP4 with the low resolution data set (28, 29). The positions of two (A and B) of the three final molecules in the asymmetric unit were found by molecular replacement. These two molecules were refined in CNS (30) and improved by iterative cycles of model building in O (31) and refinement in CNS until an R_{free} value of 35% was obtained. At this point, sparse electron density became visible for the third molecule (C). A copy of molecule A was manually inserted into the density and refined. Density for molecule C was very poor, and the B-factors were very high, so refinement was carried out using non-crystallographic restraints between the third molecule and the first molecule. Residues for molecule C, which contained no electron density, were deleted. Refinement of molecule C dropped the R_{free} to 31%. The final model was obtained by iterative cycles of model building and refinement of the three molecules against the high resolution data set. The final molecule contains residues 54–311 for molecule A and B and 54–269 and 281–311 for molecule C.

Mutational Analysis of 3-OST-1

Preparation of 3-OST-1 Mutant Plasmids—A total of 28 point mutants of 3-OST-1 were prepared using b3-OST-1-pET28 as the template and the Gene Tailor site-directed mutagenesis kit from Invitrogen. The lengths and sequences of the primers for preparation of those mutants were designed based on the manufacturer's protocol for this mutagenesis kit and were synthesized by Invitrogen. The resultant constructs were sequenced to confirm the anticipated mutation (University of North Carolina, DNA sequencing core facility).

Expression and Purification of 3-OST-1 Mutants—The expression plasmids for various 3-OST-1 mutants were transformed individually into BL21(DE3)RIL cells (Stratagene). Each mutant construct was grown in 100 ml of LB broth and induced by isopropyl-β-D-thiogalacto-

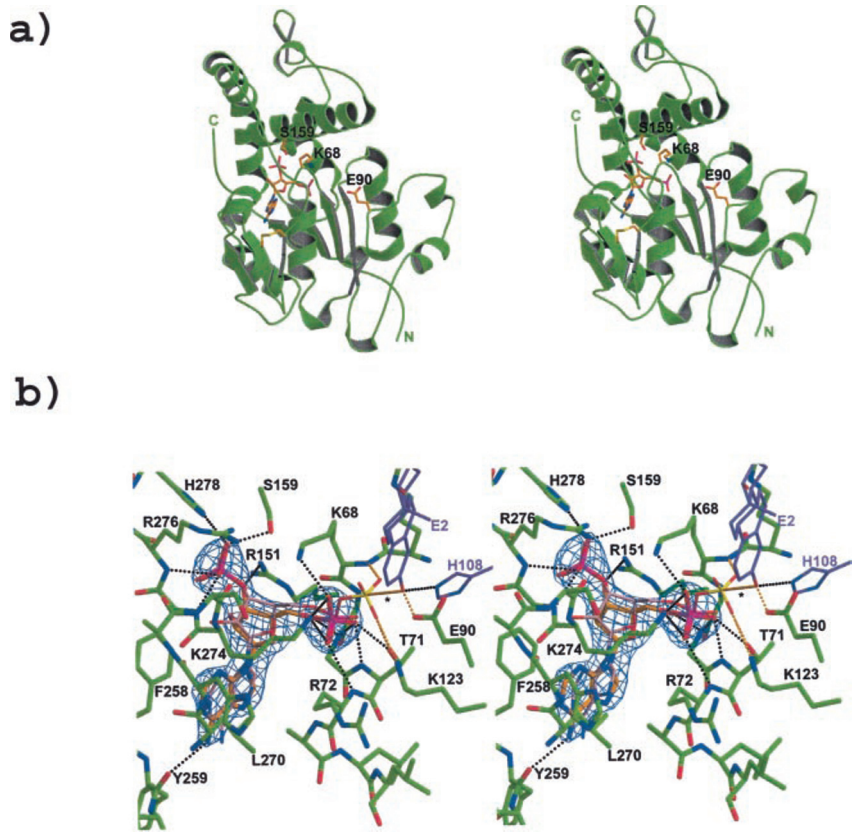

FIG. 2. **The crystal structure of 3-OST-1 in complex with PAP.** *a*, *stereo ribbon diagram* of the crystal structure of 3-OST-1. Also pictured is the donor product PAP and conserved residues Ser-159 and Lys-68 that interact with the 3′- and 5′-phosphates of PAP, respectively, as well as residue Glu-90, which has been proposed to be involved in catalysis. *b*, stereo diagram of the PAPS binding site of 3-OST-1 with PAP bound. The electron density for PAP from a simulated annealing omit map is drawn contoured at 8σ (*blue*). Superimposed onto the active site are PAPS (*pink*) from the crystal structure of human estrogen sulfotransferase (PDB code1HY3) and 17β-estradiol, the acceptor substrate, and the catalytic base His-108 (*purple*) from mouse estrogen sulfotransferase (PDB code 1AQU). Superpositions are based on the PSB loop of these structures. These superpositions suggest the position of the sulfuryl group of PAPS in 3-OST-1 binding as well as the position of the acceptor hydroxyl of the heparan substrate (the 3-hydroxyl on 17β-estradiol). Hydrogen bonds between 3-OST-1 and PAP are drawn in *dashed black lines* as well as the interaction between His-108 and 17β-estradiol in mouse estrogen sulfotransferase. Potential hydrogen bonds between 3-OST-1 residues and the sulfuryl group of PAPS are shown in *dashed orange lines* as is the potential interaction between Glu-90 and the acceptor hydroxyl of the substrate. The *solid orange line* (labeled with an *asterisk*) displays the direction of attack of the acceptor hydroxyl on the sulfuryl group for the proposed in-line transfer reaction mechanism. For this figure the oxygen, nitrogen, and phosphorous atoms are colored *red*, *blue*, and *magenta*, respectively. This figure was created using Molscript (37) and Raster3D (38).

pyranoside as described above. The bacteria cells were harvested and solubilized in sonication buffer before sonication. The lysate was subjected to a 400-μl nickel nitrilotriacetic acid-agarose column (0.75 × 1 cm) followed by a 5-ml of wash with sonication buffer. Mutant proteins were eluted with 1 ml of elution buffer containing 25 mM Tris, 500 mM NaCl, and 250 mM imidazole, pH 7.5. Approximately 25 μl of the eluent was subjected to the analysis on a 16.5% Tris-Tricine PAGE gel (Bio-Rad), and the gel was stained by Coomassie Blue. The expression level of the mutant protein was estimated by determining the intensity of the Coomassie-stained protein band near 30 kDa. As a positive control, we expressed wild type 3-OST-1 (b3-OST-1-pET28) along with the mutants. The expression levels and the sulfotransferase activity of mutant proteins were normalized to those of wild type protein.

Several clones harboring mutant proteins, including R67E, K68A, R72E, E90Q, K123A, and R276A, were grown in 2–4-liter cultures to obtain sufficient amounts of protein for analysis by isothermal titration calorimetry (ITC). Procedures for expression and purification of these mutants were essentially identical to those for the wild type 3-OST-1. Mutant protein was purified by nickel nitrilotriacetic acid-agarose chromatography, and purity was estimated to be greater than 80% by a 16.5% Tris-Tricine PAGE gel.

Determination of the Sulfotransferase Activity—Sulfotransferase activity was determined by incubating ~5 μl (10–100 ng) of purified mutant or wild type 3-OST-1 proteins with 10 μg of HS (from bovine kidney, ICN) and 5–10 × 10^4 cpm of [^{35}S]PAPS (~10 μM) in 50 μl of buffer containing 50 mM MOPS, pH 7.0, 10 mM $MnCl_2$, 5 mM $MgCl_2$, and 1% Triton X-100. The reaction was incubated at 37 °C for 30 min and quenched by the addition of 6 M urea and 100 mM EDTA. The sample was then subjected to a 200-μl DEAE-Sepharose chromatography to purify the [^{35}S]HS. The quantity of [^{35}S]HS was then determined by liquid scintillation counting. The negative control contained all the components with the exception of 3-OST-1 proteins.

Determination of the Binding of AT and 3-O-Sulfated HS—Approximately 5 × 10^6 cpm of [^{35}S]HS was incubated with 5 μg of human AT (Cutter Biological) in 50 μl of reaction buffer containing 10 mM Tris-HCl, pH 7.5, 150 mM NaCl, 1 mM Mn^{2+}, 1 mM Mg^{2+}, 1 mM Ca^{2+}, 10 μM dextran sulfate, 0.02% sodium azide, and 0.0004% Triton X-100 for 30 min at room temperature. 60 μl of 1:1 slurry of pretreated concanavalin A-Sepharose (from Sigma) was added, and the reaction was agitated for 1 h at room temperature on an orbital shaker. The gel was washed three times with the buffer containing 10 mM Tris-HCl, pH 7.5, 150 mM NaCl, 1 mM Mn^{2+}, 1 mM Mg^{2+}, 1 mM Ca^{2+}, 10 μM dextran sulfate, 0.02% sodium azide, and 0.0004% Triton X-100, and the bound [^{35}S]HS was eluted with the same buffer containing 1000 mM NaCl.

ITC—ITC was performed on a MicroCal VP-ITC. Solutions were cooled to 10 °C and degassed under vacuum before use. Experiments were conducted using 17–21 μM protein in 100 mM phosphate buffer, pH 7.0) and 100 mM NaCl at 10 °C. Titrations were performed by injecting 5 μl of 4 mM PAP in 100 mM phosphate buffer, pH 7.0, and 100 mM NaCl. Data analysis was completed using Origin software.

Determination of PAP Binding Affinity Using PAP Chromatography—To determine the binding affinity of the wild type and mutant proteins to PAP, 3′,5′-ADP-agarose chromatography (Sigma) was used. Approximately 200 μg of proteins, including wild type 3-OST-1, K68A, H92F, and D95N and R276A, in 5 ml of a buffer containing 25 mM Tris, pH 7.0, and 100 mM NaCl was loaded onto a 3′,5′-ADP-agarose column (7 × 52 mm) pre-equilibrated with 25 mM Tris, pH 7.0, and 100 mM NaCl at a flow rate of 0.5 ml/min. Unbound material was removed by

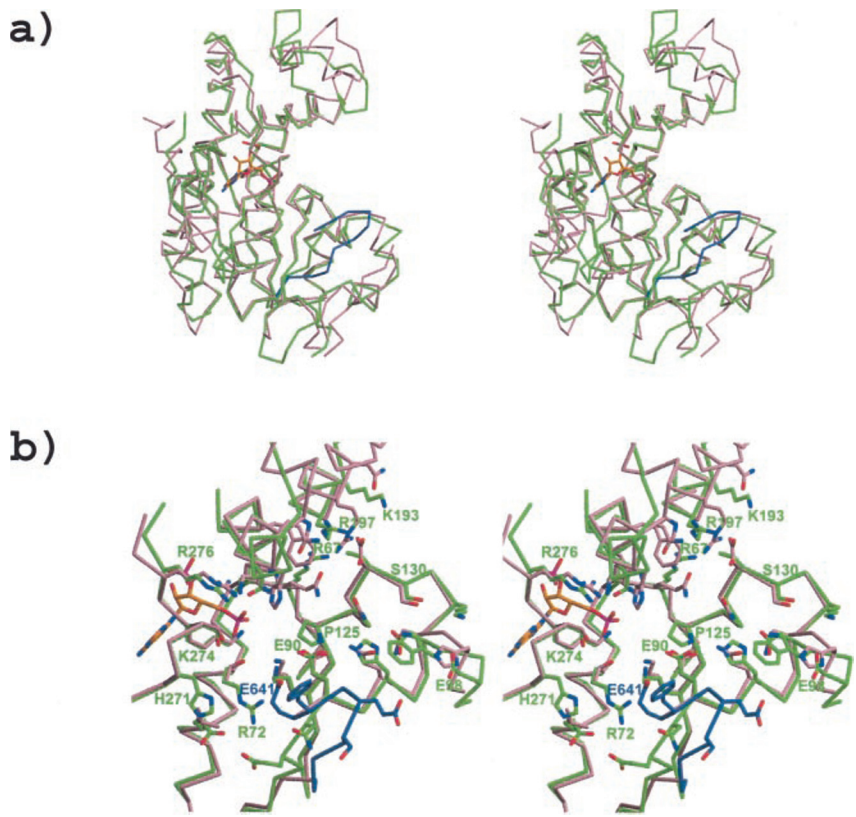

FIG. 3. **The superimposed structures of NST-1 and 3-OST-1.** *a*, stereo diagram of the Cα trace of the crystal structures of 3-OST-1 (*green*, PAP is in *orange*) with the sulfotransferase domain of NST-1 (*pink*) (PDB code 1NST). This figure clearly shows the large open cleft of the proposed heparan binding site. *b*, stereo diagram of the superposition of the active sites of 3-OST-1 and NST-1. Although the overall fold is similar, residues lining the cleft are quite different. In both *panels a* and *b* the loop unique to NST from residues 633 to 641 is colored *blue*. Glu-641 is labeled for clarity. For this figure the oxygen, nitrogen, and phosphorous atoms are colored *red*, *blue*, and *magenta*, respectively. This figure was created using Molscript (37) and Raster3D (38).

washing with 5 ml of 25 mM Tris, pH 7.0, and 100 mM NaCl. Bound proteins were eluted with a linear gradient of NaCl from 100 mM to 1 M in 10 ml. The samples from the collected fractions were analyzed by SDS-PAGE followed by staining with Coomassie Blue.

RESULTS AND DISCUSSION

Overall Fold—The catalytic domain of mouse 3-OST-1 (G48-H311) was successfully expressed in *Escherichia coli*. The catalytic domain has higher solubility than the full-length protein, making it more amenable to crystallization. The 3-OST-1 protein crystallized in the space group $I4_122$ with 3 protein molecules (A, B, and C) in the asymmetric unit. Each molecule of 3-OST-1 contains one molecule of PAP bound. Two of the protein molecules (A and B) in the asymmetric unit stack together, forming hollow channels with the long dimension running parallel to the *c* axis of the unit cell. The rim of the channel is composed of 4 molecules of both A and B. The hollow inner solvent channel has a diameter of ~62 Å. The third molecule (C) is involved in cross-linking these channels by interacting with molecules B and a molecule C coming from another channel. This packing arrangement creates a cell with an overall solvent content of 76% and a Matthews coefficient of 5.5 (32). Molecules A and B are well ordered and have similar overall B-factors (Table I). Molecule C, however, is highly disordered, with overall B-factors ~2.5 times greater than molecules A and B, suggesting it may bind in slightly different orientations or have only partial occupancy in the crystal lattice. Because molecule C is highly disordered, the discussion of the structure will focus on molecules A and B.

The crystal structure of the 3-OST-1·PAP complex (Fig. 2*a*) is roughly spherical and contains a large open cleft. The structure is centered around an α/β motif common to all sulfotransferases (18). This motif consists of a five-stranded parallel β-sheet flanked on both sides by α helices. At the heart of the fold is a strand-loop-helix motif (Thr-61–Ser-79) consisting of the first β-strand (The-61–Ile-64) and the first α-helix (Thr-71–Ser-79), which contains the phosphosulfate binding (PSB) loop (Gly-65–Gly-70) (22). This loop is very similar in structure to the P-loop found in protein kinases and forms extensive interactions with the 5′-phosphate of the PAP (Fig. 2*b*). As in other sulfotransferases, the helix that runs across the top of the PAP binding pocket and into the open cleft is also present. The C-terminal portion of the enzyme consists of a short three-

TABLE II
Distance between PAP and free SO_4^{-2} to 3-OST-1 residues

All distances are based on PAP bound to molecule B. The His-278 interaction does not exist in molecule A.

Interactions with PAP			
Residue	Atom	PAP atom	Distance
			Å
5′-Phosphate			
Lys-68	NZ	O6P	2.8
Lys-274	NZ	O6P	3.0
Gly-70	N	O4P	3.0
Thr-71	N	O4P	2.6
Thr-71	N	O4P	2.6
Arg-72	N	O5P	3.1
Lys-274	NZ	O5P	3.1
G70 Gly-70	N	O5′	3.1
3′-Phosphate			
Arg-151	NH2	O3	3.1
Ser-159	OG	O2P	2.6
His-278	NE2	O2P	3.1
Gly-275	N	O3P	2.7
Arg-276	N	O3P	3.1
Adenine base			
Tyr-259	O	N6	3.0
Interactions with free SO_4^{-2} in active site			
Residue	Atom	SO_4^{-2} atom	Distance
			Å
Arg-72	NH1	O4	2.8
Lys-123	NZ	O4	3.2
Lys-274	NZ	O3	2.8

```
3OST-1    STQQLPQTIIIGVRK GGTRALLEMLSLHPD VAAAE------NEVH FFDWEEHYSQGLGWY LTQMPFS--SPHQLT 120
3OST-5    LVQQLPKAIIIGVRK GGTRALLEMLNLHPA VVKAS------QEIH FFDNDENYGKGIEWY RKKMPFS--YPQQIT 152
3OST-3A   GSKQLPQAIIIGVKK GGTRALLEFLRVHPD VRAVG------AEPH FFDR--SYDKGLAWY RDLMPRT--LDGQIT 212
NST-1     TCDRFPKLLIIGPQK TGTTALYLFLGMHPD LSSNYPSSETFEEIQ FFNG-HNYHKGIDWY MEFFPIPSNTTSDFY 673
                                            *** *

3OST-1    VEKTPAYFTSPKVPE RIHSMNPTIRLLLIL RDPSERVLSDYTQVL YNHLQKHKPYPPIED LLMRD----GRLNLD 191
3OST-5    IEKSPAYFITEEVPE RIYKMNSSIKLLIIV REPTTRAISDYTQVL EGKERKNKTYYKFEK LAIDPN--TCEVNTK 225
3OST-3A   MEKTPSYFVTREAPA RISAMSKDTKLIVVV RDPVTRAISDYTQTL S----KRPDIPTFES LTFKNRT-AGLIDTS 282
NST-1     FEKSANYFDSEVAPR RAAALLPKAKVLTIL INPADRAYSWYQHQR AHDDPVAL-KYTFHE VITAGSDASSKLRAL 747
                                          *  *    *

3OST-1    -YKALNRSLYHAHML NWLRFFPLGHIHIVD GDRLIRDPFPEIQKV ERFLKLS-PQINASN FYFNKTKGFYCLRD- 263
3OST-5    -YKAVRTSIYTKHLE RWLKYFPIEQFHVVD GDRLITEPLPELQLV EKFLNLP-PRISQYN LYFNATRGFYCLRFN 298
3OST-3A   -WSAIQIGIYAKHLE HWLRHFPIRQMLFVS GERLISDPAGELGRV QDFLGLK-RIITDKH FYFNKTKGFPCLKKA 355
NST-1     QNRCLVPGWYATHIE RWLSAYHANQILVLD GKLLRTEPAKVMDMV QKFLGVTNTIDYHKT LAFDPKKGFWCQLLE 821

                                                                                  %identity
3OST-1    --SGKDRCLHESKGR AHPQVDPKLLDKLHE YFHEPNKKFFKLVGR TFDWH---------- -- 311      -
3OST-5    --IIFNKCLAGSKGR IHPEVDPSVITKLRK FFHPFNQKFYQITGR TLNWP---------- -- 346      53
3OST-3A   EGSSRPHCLGKTKGR THPEIDREVVRRLRE FYRPFNLKFYQMTGH DFGWDG--------- -- 406      43
NST-1     --GGKTKCLGKSKGR KYPEMDLDSRAFLKD YYRDHNIELSKLLYK MGQTLPTWLREDLQN TR 882      28
```

FIG. 4. **Alignment of mouse 3-OST-1 with human 3-OST-5, 3-OST-3A, and NST-1.** NST-1 alignment is based on the structural alignment with 3-OST-1. Regions with *yellow background* are structurally dissimilar. Mutants of residues in *red*, knockout activity in 3-OST-1, <2% WT activity (*orange*), <10% WT (*green*), and >10% WT (*blue*). Residues in *purple* form a disulfide bond. NST-1 amino acids labeled by a *red asterisk* indicate amino acid mutants with no activity, and *green asterisk*-labeled residues have greatly reduced activity (results are taken from Kakuta *et al.* (34)). The percentage of amino acid identity with 3-OST-1 is shown in the *bottom right corner* of this figure.

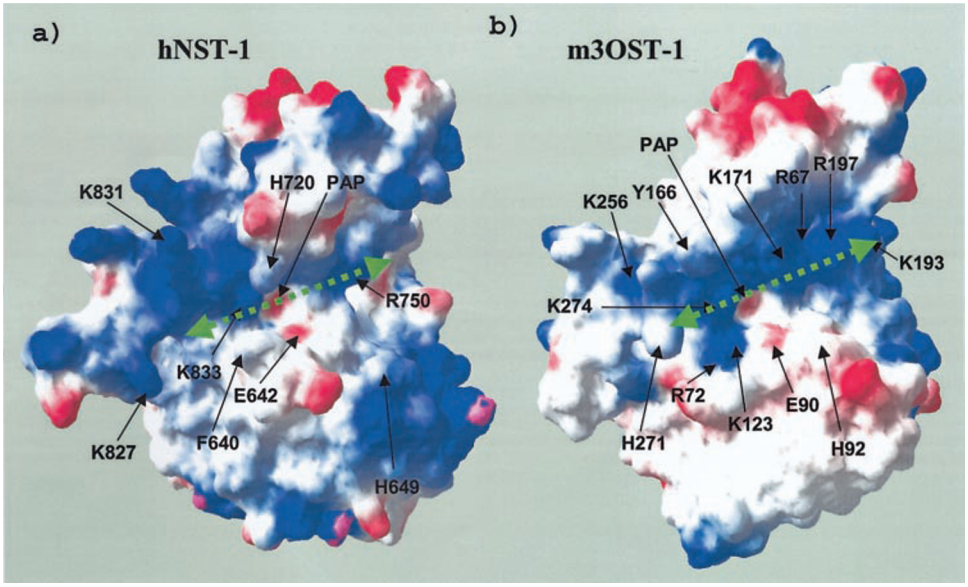

FIG. 5. **Charged surface diagram of the proposed heparan binding cleft of the sulfotransferase domains of NST-1 (*a*) and 3-OST-1 (*b*).** The global position of the cleft is marked with a *green dashed line*. Blue surfaces signify positive charge, whereas *red* surfaces signify negative charge. The *double-sided dash arrows* (in *green*) indicate the region where HS may bind. This figure was created using Swiss PDB viewer.

stranded anti-parallel β-sheet. Strands 2 and 3 of this sheet are stabilized by a disulfide bond (Cys-260–Cys-269). A coil consisting of residues 270–281 connects this sheet to the C-terminal helix. This coil practically buries the PAP molecule in the active site and may be susceptible to a conformational change since it is ordered in molecules A and B and there is no electron density visible for it in molecule C.

The overall fold of 3-OST-1 is most similar to that of the sulfotransferase domain of NST-1 (21) (Fig. 3*a*). The root mean square of 230 structurally equivalent Cαs is 1.3 Å, as determined by the program O (31). All of the significant secondary structural features are conserved between the two enzymes. The major differences occur in the loop regions as described below.

PAP Binding Site—A number of hydrogen-bonding interactions are involved in positioning the PAP molecule within the active site (Fig. 2*b*). Side chains from residues Lys-68 and Thr-71 of the PSB loop and Lys-274 of the coil that buries the PAP both form interactions with the 5′-phosphate (Table II). In addition, backbone amide nitrogens from the PSB loop (Gly-70, Thr-71, and Arg-72) are also within hydrogen-bonding distance of the 5′-phosphate. Although there are no protein interactions with the ribose ring, atom N6 of the adenosine base is within hydrogen-bonding distance to the carbonyl oxygen of Tyr-259. In addition, residues Phe-258, Ile-225, Ala-73, and Leu-270 are all within 4 Å of the base and assist in positioning the base through van der Waals forces.

Like the 5′-phosphate binding site, the 3′-phosphate also forms a number of interactions with the protein. The side chain of Arg-151 is within hydrogen-bonding distance to the bridging O3 oxygen. In addition, the side chain oxygen of Ser-159 also lies within hydrogen-bonding distance of Arg-151 as well as

TABLE III
Summary of the analysis of 3-OST-1 mutants

The wild type m3-OST-1 was constructed by replacing N-terminal 47 amino acid residues with a His_6 tag to facilitate the protein purification.

Name of the constructs[a]	Expression level[b]	Relative activity[c]
		%
3-OST-1 wild type	+	100.0
3-OST-1 R67E	+	1.1
3-OST-1 R67A	+	1.2
3-OST-1 K68A	++	0.1
3-OST-1 R72A	++	7.0
3-OST-1 R72E	++	0.0
3-OST-1 E76A	+	30.7
3-OST-1 E76Q	+	15.6
3-OST-1 E88A	+	63.7
3-OST-1 N89A	+	69.5
3-OST-1 N89D	+	74.4
3-OST-1 E90Q	+	<0.0
3-OST-1 E90A	+	0.0
3-OST-1 H92F	+	<0.0
3-OST-1 H92A	+	0.0
3-OST-1 D95A	Somewhat lower than WT, detectable	<0.0
3-OST-1 D95N	Somewhat lower than WT, detectable	8.1
3-OST-1 W96A	+	91.6
3-OST-1 W96F	+	69.1
3-OST-1 E98A	+	65.6
3-OST-1 K123A	++	0.2
3-OST-1 K132A	+	49.1
3-OST-1 R197A	++	95.0
3-OST-1 Q163A	++	34.0
3-OST-1 H271A	++	109.0
3-OST-1 H271F	++	42.0
3-OST-1 S273A	+	99.6
3-OST-1 K274A	+	17.4
3-OST-1 R276A	+	0.3

[a] The mutants were prepared using site-directed mutagenesis kit from Invitrogen. The constructs were sequenced to confirm the point mutations. The proteins were expressed in *E. coli* and purified by a nickel nitrilotriacetic acid-agarose column.

[b] The expression level of the proteins was determined by the intensity of the Coomassie Blue-stained protein band migrated at 30 kDa on SDS-PAGE.

[c] The activity of 3-OST-1 was determined by following a method described in a prior publication (39), and 100% activity represents the transfer of 14 pmol of sulfate/μg of protein under the standard assay condition.

with a 3′-phosphate oxygen. Backbone amides from residues Gly-275 and Arg-276 of the flexible loop also form interactions with the phosphate. In molecule B, atom NE2 of the side chain from His-278 is within hydrogen-bonding distance of the phosphate as well; however, this residue has a different conformation in molecule A and consequently is not near the phosphate.

Catalytic Mechanism—Heparan sulfotransferases, including 3-OST-1 and NST-1, and cytosolic sulfotransferases recognize substrates that have distinct chemical structures. Based on structural similarities and utilization of the same sulfuryl donor, PAPS, it is believed that heparan sulfotransferases and cytosolic sulfotransferases share a common mechanism (33). Superposition of 3-OST-1 with structures of estrogen sulfotransferase, a representative cytosolic sulfotransferase, with PAPS and 17β-estradiol bound depicts the catalytic functions of the key amino acid residues for the activities of 3-OST-1 and estrogen sulfotransferase (Fig. 2*b*). The mechanism of the cytosolic sulfotransferases has been suggested to proceed through an S_N2-like in-line displacement mechanism whereby the acceptor hydroxyl acts as a nucleophile, which when deprotonated by a conserved histidine attacks the sulfur atom of PAPS (20, 22). This creates a trigonal bi-pyramidal transition state with the PAP and acceptor group in the axial positions. The negative charge build up on the leaving PAP group is stabilized by a conserved lysine residue on the PSB loop that forms a hydrogen bond with the bridging oxygen to the sulfur atom. This lysine is in a similar conformation in both the structures of estrogen sulfotransferase in complex with PAP and 17β-estradiol and 3-OST-1 in complex with PAP. Interestingly, in the estrogen sulfotransferase-PAPS binary complex, the lysine lies in a different conformation and forms a hydrogen bond with a conserved serine that also forms hydrogen bonds with the 3′-phosphate of PAP (24). This interaction may be essential for all sulfotransferases to reduce the rate of hydrolysis of PAPS in the absence of acceptor substrate.

The lysine and serine residues, which are used by estrogen sulfotransferase to position and stabilize PAPS, are conserved in NST-1 (Lys-614, Ser-712) as well as in the 3-OSTs including 3-OST-1 (Lys-68, Ser-159, respectively) (Fig. 2*b*). The catalytic base, however, is not conserved between the estrogen sulfotransferase and the heparan sulfotransferases. The heparan sulfotransferases do not contain a residue structurally equivalent to the catalytic histidine found in cytosolic sulfotransferases such as the estrogen sulfotransferases. However, a conserved glutamate is located at a different position in the catalytic sites of NST-1 (Glu-642) and 3-OST-1 (Glu-90) (Fig. 2*b*). This glutamate residue was proposed to serve as the catalytic base for the activity of NST-1 (33, 34). In both 3-OST-1 and NST-1 structures, this glutamate is found on the inside of the large cleft. Mutation at Glu-90 of 3-OST-1 results in complete loss of sulfotransferase activity as described below, suggesting that Glu-90 is critical for the catalytic function of 3-OST-1.

Heparan Sulfate Binding Site—The large open cleft of the 3-OST-1 structure is believed to be the HS binding site (Fig 3*a*). This hypothesis is based on the fact that this open cleft in NST-1 has been shown to accommodate a hexasaccharide and provides access to the sulfuryl group of PAPS, where the sulfotransfer reaction occurs (34). Despite the overall fold of these two enzymes being similar, the cleft of 3-OST-1 differs from that of NST-1 in both the primary amino acid sequence and the distribution of the positively charged amino acid residues. NST-1 contains an insertion immediately before the catalytic base (residues Asn-633—Glu-641) that does not exist in 3-OST-1 molecules (Figs. 3*b* and 4). Mutations from this loop F640A and E641A have a significant effect on NST-1 activity (34). Because these residues are not conserved in the 3-OSTs, it is unlikely that this loop of NST-1 plays a fundamental role in catalysis of all HS sulfotransferase reaction. Therefore, it is possible that this NST-1-specific loop helps the enzyme to recognize NST-1-specific saccharide units within its polysaccharide substrate (the structures of NST-1 and 3-OST-1 substrates are shown in Fig. 1).

The majority of the residues that line this cleft are not conserved. An increase in overall positive charge of the surface of the 3-OST-1 cleft as compared with the NST-1 cleft (Fig. 5) is consistent with the greater number of sulfo groups on the 3-OST-1 substrate than found on the NST-1 substrate (Fig. 1). Interestingly, additional electron density was found in the electron density maps of 3-OST-1 that we have modeled as inorganic sulfate. Residues Arg-72, Lys-123, and Lys-274 are all within hydrogen-bonding distance to the modeled inorganic sulfate (Table II). The position of this modeled inorganic sulfate may represent a sulfo group binding site for the HS substrate, conferring specificity for the 3-OSTs. Consistent with this observation, mutations of Lys-123 and Arg-72 (described below) result in a significant reduction of the sulfotransferase activity (Table III).

Mutational Analysis of 3-OST-1—Site-directed mutagenesis experiments were performed to help determine which amino acid residues might be involved in PAPS binding, HS binding, and/or catalysis. Eighteen different amino acid residues within

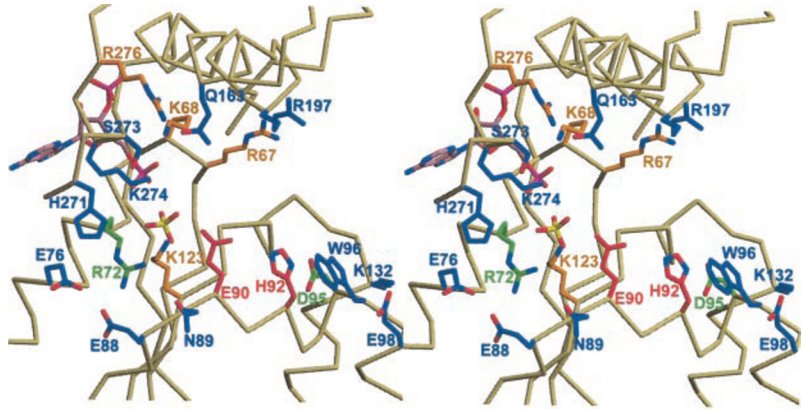

FIG. 6. **Stereo diagram of the heparan binding cleft of 3-OST-1.** Residues that have been mutated in this study are shown. Mutations of residues in *red* abolish activity, whereas mutations of residues in *orange* reduce the activity to <2% of wild type. Mutations of residues in *green* reduce the activity to <10% of wild type. Mutations of residues in *blue* do not significantly affect activity. For this figure the oxygen, nitrogen, and phosphorous atoms are colored *red*, *blue*, and *magenta*, respectively. This figure was created using Molscript (37) and Raster3D (38).

TABLE IV
Comparison of the thermodynamic parameters of PAP to 3-OST-1 WT and 3-OST-1 mutants as determined by ITC analysis

Protein	K_D	Number of binding sites	ΔH	ΔS
	μM	*n*	*cal/mol*	*cal/mol*
WT	14 ± 4	0.8 ± 0.2	−1081 ± 315	18.4
R67E	18 ± 5	0.89 ± 0.19	−2455 ± 600	13.0
K68A[a]	N/A[b]	N/A	N/A	N/A
R72E	5.2 ± 0.8	0.8 ± 0.04	−3234 ± 209	12.7
E90Q	5.5 ± 2	0.68 ± 0.27	−868 ± 428	21.0
K123A	11 ± 2	0.72 ± 0.07	−2179 ± 251	14.9
R276A[a]	N/A	N/A	N/A	N/A

[a] Due to the low binding affinities between the mutants and PAP, the amount of heat release was low under the experimental conditions. Thus, the appropriate curve fitting analysis for obtaining the K_D was not feasible.
[b] N/A, not applicable.

and around the PAPS binding site and the proposed HS binding cleft were mutated. The results of the mutagenesis study are summarized in Table III. The positions of the mutation sites at the active site of 3-OST-1 are shown in Fig. 6. Binding of enzymatically modified HS to AT were compared in those mutants that retained sulfotransferase activity. HS modified by all of these mutants bound to AT, suggesting that these mutant proteins maintain the substrate specificity of 3-OST-1 (data not shown). Point mutations in residues 67, 68, 72, 90, 92, 95, 123, and 276 abolish or significantly reduce the enzymatic activity, suggesting that these residues are essential for sulfotransferase activity.

To help decipher the specific roles of these individual amino acids in catalysis, binding affinity for PAP was measured and compared with wild type using ITC analysis (Table IV). The use of PAP as an analog for mimicking the interaction between PAPS and sulfotransferases is a widely used approach, provided that the binding affinity of sulfotransferases to PAP is similar to the affinity of sulfotransferase to PAPS (18). Indeed, we determined the K_D of 3-OST-1 (WT) for PAP to be 14 μM, very close to the 10 μM K_m of wild type 3-OST-1 for PAPS, determined by kinetic analysis (35). Our result suggests that the PAP binding affinity of 3-OST-1 provides a good estimate for the binding affinity to PAPS. The binding affinity (K_D values) of the protein to PAP among the mutants K123A, R67E, E90Q, and R72E is similar to the wild type protein, suggesting that residues Arg-67, Arg-72, Glu-90, and Lys-123 are not directly involved in the binding to PAP.[2] However, we were unable to accurately determine the K_D values for mutants K68A and mutant R276A because the binding affinity is too low. We next compared the binding/elution profiles of these proteins on a PAP-agarose column. We find that the wild type 3-OST-1 protein was eluted from the column at 1 M NaCl, whereas 3-OST-1 K68A and 3-OST-1 R276A were eluted at 600 and 150 mM NaCl, respectively (chromatograms not shown). These results suggest that the PAP binding affinities of 3-OST-1 K68A and 3-OST-1 R276A are indeed significantly reduced. The decrease in the PAP binding affinity of mutant K68A is consistent with our crystal structure data that reveals the side chain of Lys-68 is in position to form a hydrogen bond with the 5′-phosphate of PAP. However, the reason for a decrease in the PAP binding affinity of mutant R276A is unclear since the side chain of this arginine residue points away from both the 3′-phosphate and 5′-phosphate of PAP.

Among those mutants that have a significant decrease in activity, Glu-90 and Lys-123 of 3-OST-1 are conserved in NST-1 (Glu-642 and Lys-676, respectively) and other 3-OSTs, suggesting that these two residues serve similar functions for the activities of these HS sulfotransferases. As described above, the proposed function of Glu-90 of 3-OST-1 or Glu-642 of NST-1 is to serve as a catalytic base in an S_N2-like in-line displacement reaction. Indeed, mutations in Glu-642 of NST-1 and Glu-90 of 3-OST-1 abolished sulfotransferase activity (34). The crystal structure data suggest that Lys-123 in 3-OST-1 is in a position to interact with the sulfo group of PAPS (Fig. 2*b*). This interaction has also been suggested to occur in NST-1 (Lys-676) based on modeling of PAPS into the active site (33). It is possible that the role of Lys-123 is not to increase binding affinity for PAPS but rather to assist in stabilizing the transition state by interacting with the equatorial oxygen atoms of the sulfo group.

Several amino acid residues critical for the sulfotransferase activity of 3-OST-1 are conserved in other 3-OST isoforms, including 3-OST-1, -2, -3, -4, and -5, but are not conserved in NSTs (36) (Fig. 4). These residues include Arg-67, Arg-72,

[2] We were unable to obtain sufficient amount purified 3-OST-1 H92F, 3-OST-1 D95A, and 3-OST-1 D95N mutants for ITC analyses. However, we purified sufficient amount of the mutant proteins to obtain the elution profiles from PAP-agarose chromatography. Both 3-OST-1 H92F and 3-OST-1 D95N were eluted from the column at 1 M NaCl, suggesting that the mutants have similar binding affinity to PAP as that of wild type protein.

His-92, and Asp-95.[3] This observation suggests that these residues contribute to the substrate specificity of 3-*O*-sulfotransferases. At the present time, it is unclear how these amino acid residues contribute to the substrate specificity, namely how 3-OST sulfonates the 3-OH position, whereas NST sulfonates the 2-amino position of the glucosamine unit. In addition, a possible catalytic role for residues His-92 and Asp-95 cannot be ruled out. Atom NE2 of His-92 from 3-OST-1 is only 3.3 Å away from a carboxylate oxygen atom of the proposed base Glu-90. Additionally, Asp-95 forms a hydrogen bond with ND1 of His-92. This sequence of residues (Glu-90– His-92–Asp-95) provides for a potential hydrogen-bonding network. Supporting this hypothesis, the mutant D95N, which could geometrically maintain the hydrogen-bonding network, does retain some sulfotransferase activity, whereas the D95A mutant does not (Table III). Interestingly in NST-1, Gln-644 is within hydrogen-bonding distance of Glu-642 (3.1 Å) the proposed base. The mutant Q644A also shows a significant loss of activity, suggesting a similar role to His-92 in 3-OST-1 for catalytic function. This proposed hydrogen bonding network could either provide activation for the glutamate as the base for catalysis or simply play a structural role by orienting the base in the proper conformation for catalysis.

The positions of residues Arg-67 and Arg-72 do not appear to support a role in catalysis. In NST-1, the corresponding residues are Gln-613 and Thr-618, respectively. The positive charge on these arginine residues in 3-OST-1 may assist in the interaction of these residues with negatively charged sulfo groups on the HS substrate. As previously mentioned, Arg-72 lies within hydrogen-bonding distance of the free inorganic sulfate modeled into the electron density. To fully understand the role of these residues and others in 3-OST-1 substrate binding, a ternary complex with both HS and PAP bound to 3-OST-1 will be required.

In conclusion, we have presented the results from the study of a crystal structure of the binary complex of 3-OST-1 and PAP and mutational analysis. Comparing the current structure of 3-OST-1 with the previously published structure of NST-1, several amino acid residues have been identified that may play a role in directing the substrate specificity of HS sulfotransferases. Because 3-OST is present in six different isoforms and the 3-OST-modified HS pose distinct biological activities, a remaining challenge is to understand the mechanism employed by the different isoforms to distinguish the saccharide sequence of their unique substrates. From the present study we are unable to reveal the precise molecular details of the substrate specificity differences between the 3-OSTs. Although the present study does not reveal the mechanism of substrate specificity differences between the 3-OSTs, the results from this study provide valuable structural information toward a comprehensive understanding of HS biosynthesis.

Acknowledgments—We thank Dr. Ashutosh Tripathy (University of North Carolina, Macromolecular Interaction Facility) for the assistance with isothermal titration calorimetry study, Dr. Joe Krahn for help in structure determination, Dr. Z. Jin of SER-CAT for collection of the data, and Drs. Jeffrey Boyington and Lee G. Pedersen as well as Andrea Moon for critical reading of the manuscript. Use of the Advanced Photon Source was supported by the United States Department of Energy, Office of Science, Office of Basic Energy Sciences under Contract W-31-109-Eng-38.

[3] The corresponding amino acid residue for Arg-67 of 3-OST-1 in 3-OST-2, 3-OST-3, and 3-OST-5 are Lys-113, Lys-136, and Arg-99, respectively. The corresponding amino acid residue for 3-OST-4 is not published.

REFERENCES

1. Esko, J. D., and Selleck, S. B. (2002) *Annu. Rev. Biochem.* **71,** 435–471
2. Rosenberg, R. D., Showrak, N. W., Liu, J., Schwartz, J. J., and Zhang, L. (1997) *J. Clin. Investig.* **99,** 2062–2070
3. Liu, J., and Thorp, S. C. (2002) *Med. Res. Rev.* **22,** 1–25
4. Lindahl, U., Kusche-Gullberg, M., and Kjellen, L. (1998) *J. Biol. Chem.* **273,** 24979–24982
5. Kuberan, B., Lech, M. Z., Beeler, D. L., Wu, Z. L., and Rosenberg, R. D. (2003) *Nat. Biotechnol.* **21,** 1343–1346
6. Atha, D. H., Lormeau, J.-C., Petitou, M., Rosenberg, R. D., and Choay, J. (1985) *Biochemistry* **24,** 6723–6729
7. Dewerchin, M., Herault, J.-P., Wallays, G., Petitou, M., Schaeffer, P., Millet, L., Weitz, J. I., Moons, L., Collen, D., Carmeliet, P., and Herbert, J.-M. (2003) *Cir. Res.* **93,** 1120–1126
8. Koide, T., Odani, S., Takahashi, K., Ono, T., and Sakuragawa, N. (1984) *Proc. Natl. Acad. Sci. U. S. A.* **81,** 289–293
9. van Boven, H. H., and Lane, D. A. (1997) *Semin. Hematol.* **34,** 188–204
10. Boyer, C., Wolf, M., Vedrenne, J., Meyer, D., and Larrieu, M. J. (1986) *Thromb. Haemostasis* **56,** 18–22
11. Weitz, J. I. (2003) *J. Clin. Investig.* **111,** 952–954
12. Liu, J., Shworak, N. W., Fritze, L. M. S., Edelberg, J. M., and Rosenberg, R. D. (1996) *J. Biol. Chem.* **271,** 27072–27082
13. Duncan, M. B., Chen, J., Krise, J. P., and Liu, J. (2004) *Biochim. Biophys. Acta* **1671,** 34–43
14. HajMohammadi, S., Enjyoji, K., Princivalle, M., Christi, P., Lech, M., Beeler, D. L., Rayburn, H., Schwartz, J. J., Barzegar, S., de Agostini, A. I., Post, M. J., Rosenberg, R. D., and Shworak, N. W. (2003) *J. Clin. Investig.* **111,** 989–999
15. Liu, J., and Rosenberg, R. D. (2002) in *Handbook of Glycosyltransferases and Their Related Genes* (Taniguchi, N., and Fukuda, M., eds) pp. 475–483, Springer-Verlag, Tokyo
16. Xia, G., Chen, J., Tiwari, V., Ju, W., Li, J.-P., Malmström, A., Shukla, D., and Liu, J. (2002) *J. Biol. Chem.* **277,** 37912–37919
17. Shukla, D., Liu, J., Blaiklock, P., Shworak, N. W., Bai, X., Esko, J. D., Cohen, G. H., Eisenberg, R. J., Rosenberg, R. D., and Spear, P. G. (1999) *Cell* **99,** 13–22
18. Negishi, M., Pedersen, L. G., Petrotchenko, E., Shevtsov, S., Gorokhov, A., Kakuta, Y., and Pedersen, L. C. (2001) *Arch. Biochem. Biophys.* **390,** 149–157
19. Grunwell, J. R., and Bertozzi, C. R. (2002) *Biochemistry* **41,** 13117–13126
20. Kakuta, Y., Pedersen, L. G., Carter, C. W., Negishi, M., and Pedersen, L. C. (1997) *Nat. Struct. Biol.* **4,** 904–908
21. Kakuta, Y., Sueyoshi, T., Negishi, M., and Pedersen, L. C. (1999) *J. Biol. Chem.* **274,** 10673–10676
22. Kakuta, Y., Petrotchenko, E. V., Pedersen, L. C., and Negishi, M. (1998) *J. Biol. Chem.* **273,** 27325–27330
23. Lee, K. A., Fuda, H., Lee, Y. C., Negishi, M., Strott, C. A., and Pedersen, L. C. (2003) *J. Biol. Chem.* **278,** 44593–44599
24. Pedersen, L. C., Petrotchenko, E., Shevtsov, S., and Negishi, M. (2002) *J. Biol. Chem.* **277,** 17928–17932
25. Shworak, N. W., Liu, J., Fritze, L. M. S., Schwartz, J. J., Zhang, L., Logeart, D., and Rosenberg, R. D. (1997) *J. Biol. Chem.* **272,** 28008–28019
26. Bame, K. J., and Esko, J. D. (1989) *J. Biol. Chem.* **264,** 8059–8065
27. Otwinowski, Z., and Minor, V. (1997) *Methods Enzymol.* **276,** 307–326
28. Bailey, S. (1994) *Acta Crystallogr. Sect. D* **50,** 760–763
29. Vagin, A., and Teplyakov, A. (1997) *J. Appl. Crystallogr.* **30,** 1022–1025
30. Brunger, A. T., Adams, P. D., Clore, G. M., DeLano, W. L., Gros, P., Grosse-Kunstleve, R. W., Jiang, J. S., Kuszewski, J., Nilges, M., Pannu, N. S., Read, R. J., Rice, L. M., Simonson, T., and Warren, G. L. (1998) *Acta Crystallogr. Sect. D* **54,** 905–921
31. Jones, T. A., Zou, J. Y., Cowan, S. W., and Kjeldgaard, M. (1991) *Acta Crystallogr. Sect. A* **47,** 110–119
32. Matthews, B. W. (1968) *J. Mol. Biol.* **33,** 491–497
33. Gorokhov, A., Perera, L., Darden, T. A., Negishi, M., Pedersen, L. C., and Pedersen, L. G. (2000) *Biophys. J.* **79,** 2909–2917
34. Kakuta, Y., Li, L., Pedersen, L. C., Pedersen, L. G., and Negishi, M. (2003) *Biochem. Soc. Trans.* **31,** 331–334
35. Myette, J. R., Shriver, Z., Liu, J., Venkataraman, G., Rosenberg, R., and Sasisekharan, R. (2002) *Biochem. Biophys. Res. Commun.* **290,** 1206–1213
36. Shworak, N. W., Liu, J., Petros, L. M., Zhang, L., Kobayashi, M., Copeland, N. G., Jenkins, N. A., and Rosenberg, R. D. (1999) *J. Biol. Chem.* **274,** 5170–5184
37. Kraulis, P. J. (1991) *J. Appl. Crystallogr.* **24,** 946–950
38. Merritt, E. A., and Bacon, D. J. (1997) *Methods Enzymol.* **277,** 505–524
39. Chen, J., Duncan, M. B., Carrick, K., Pope, M., and Liu, J. (2003) *Glycobiology* **13,** 785–794